

Supplementary Material

Oxygen-Vacancy Enhanced CoO/CeO₂ Heterojunction for Synchronous Regulation of Sulfur Resourcing and Selenium Adsorption Separation from Flue Gas Desulfurization Wastewater

Tieyue Qi^{a,b,§}, Xi Chen^{a,b,§}, Jingzhao Zhang^{a,b}, Jiabin Gao^{a,b}, Runlong Hao^{a,b,*}, John Crittenden^c

a Hebei Key Laboratory of Power Plant Flue Gas Multi-Pollutants Control, Department of Environmental Science and Engineering, North China Electric Power University, Baoding, 071003, China

b MOE Key Laboratory of Resources and Environmental Systems Optimization, College of Environmental Science and Engineering, North China Electric Power University, Beijing, 102206, China

c Brook Byer Institute for Sustainable Systems and School of Civil and Environmental Engineering, Georgia Institute of Technology, Atlanta, Georgia 30332, United States;

§ indicates the co-first author.

** Corresponding authors E-mail: hrl_ncepu@hotmail.com*

Submitted to
Journal of Materials Chemistry A

Number of pages (including this page): 42

Number of texts: 6

Number of figures: 20

Number of tables: 11

Texts

Text S1 Chemicals and materials

All reagents were used directly without further purification. Cobalt nitrate hexahydrate ($\text{Co}(\text{NO}_3)_2 \cdot 6\text{H}_2\text{O}$, 99%, Macklin Co., China.) and urea (H_2NCONH_2 , 99%, Kermel Co., China.) were used to synthesize cobalt carbonate via hydrothermal method. Cerium nitrate ($\text{Ce}(\text{NO}_3)_2 \cdot 6\text{H}_2\text{O}$, 99%, Macklin Co., China.) and polyvinylpyrrolidone (PVP, 99%, Kermel Co., China.) were used to synthesize CoO/CeO_2 catalysts. In addition, ethanol ($\text{C}_2\text{H}_5\text{OH}$, 99.7%, Damao Technology Co., China) and deionized (DI) water obtained from Milli-Q ultrapure water purification system (Millipore, Billerica, MA) were used as washing solution. Sodium borohydride (NaBH_4 , 99%, Damao Technology Co., China.) was used to establish oxygen vacancies on the catalysts. Sulfite (Na_2SO_3 , 97%, Damao Technology Co., China.) and selenium (Se, 1000ug/mL in 2.0 mol/L HNO_3 , Aladdin Co., China.) were used as the target pollutants. HCl (36-38%wt, Damao Co. Technology Co., China.), thiourea ($\text{CH}_4\text{N}_2\text{S}$, 99%, Kermel Co., China.) and L-ascorbic acid (99.7%, Kermel Co., China.) were used as the reducing solution to when testing the concentration of Se. Sodium hydroxide (NaOH , 99%, Damao Co. Technology Co., China.) and HCl were used to adjust the pH of mixture solution. A commercial polytetrafluoroethylene (PTFE) microfiltration membrane ($\Phi=50$ mm, pore diameter=0.45 μm) was used to collect products by filtration.

Text S2. Adsorption Kinetics

To reveal the behavior and mechanism of Se adsorption, the Se adsorption kinetics were further studied based on the pseudo-first-order model, pseudo-second-order model and intra-particle diffusion model.¹⁻³ The related parameters are summarized in Table S2. The fitting result shown in Fig. S3 indicates that the pseudo-first-order model is not fit. By contrast, as shown in Fig. S4, the regression coefficients (R^2) of the pseudo-second-order fitting curve for all materials are close to 1, and the $q_{e,cal}$ values are well agree with the experimental q_e values, demonstrating that pseudo-second-order model is competent to describe the adsorption kinetics of Se.

In addition, the intra-particle diffusion model was also employed to determine the rate-determining step in Se adsorption process. As shown in Fig. S5, the Se adsorption process can be divided into three linearity plots, i.e. external transfer step, intra-particle diffusion step and final equilibrium step⁴⁻⁶; and the plots of q_t against $t^{1/2}$ are straight lines passing through the origin, indicating that the rate-determining step is pore diffusion rather than boundary layer diffusion^{2,4}.

$$\frac{1}{q_t} = \frac{k_1}{q_{e1}t} + \frac{1}{q_{e1}} \quad (1)$$

$$\frac{t}{q_t} = \frac{1}{(k_2q_{e2}^2)} + \frac{t}{q_{e2}} \quad (2)$$

$$q_t = k_{id}t^{1/2} + I \quad (3)$$

where k_1 and k_2 are the pseudo-first-order constant and pseudo-second-order constant, respectively; R^2 is the linear correlation coefficient; q_e ($\text{mg}\cdot\text{g}^{-1}$) represents the adsorption capacity of the adsorbent at equilibrium; q_t ($\text{mg}\cdot\text{g}^{-1}$) is the adsorption capacity of the adsorbent at time t ; K_{id} ($\text{mg}\cdot\text{g}^{-1}\cdot\text{min}^{-1/2}$) denotes the intra-particle diffusion rate constant; and I is the intercept of the intra-particle diffusion model.

Text S3. Adsorption Isotherm

To further determine the adsorption capacity of Se, the adsorption isotherms were established according to the Langmuir and Freundlich isotherm models, with the initial concentration of Se ranging from 0 to 200 mg/L. Table S4 summarizes the parameters of Langmuir and Freundlich isotherms. As shown in Fig. S6, Se adsorption capacity increases constantly with the increase in equilibrium concentration (C_e), and reaches saturation in the end, with the maximum adsorption capacity of higher than 120 mg/g. Moreover, the R^2 of Freundlich model is higher than that of Langmuir model, so Se adsorption process follows the Freundlich model. Herein, the fitting results of kinetic and isotherm adsorption curves suggested that the mechanism of Se adsorption was involved with chemisorption on multilayers⁵.

$$q_e = \frac{q_{max}K_L C_e}{1 + K_L C_e} \quad (4)$$

$$q_e = K_F C_e^{1/n} \quad (5)$$

where C_e ($\text{mg}\cdot\text{L}^{-1}$) represents the equilibrium concentration of Se in solution; q_e ($\text{mg}\cdot\text{g}^{-1}$) is the amount of adsorbed Se per unit mass of the 70 wt% OV-CoO/CeO₂ composite material; K_L ($\text{L}\cdot\text{mg}^{-1}$) denotes Langmuir affinity constant related to the energy of adsorption; q_{max} ($\text{mg}\cdot\text{g}^{-1}$) is the maximum adsorption capacity; K_F ($\text{mg}/\text{g}\cdot(\text{L}/\text{mg})^{1/n}$) represents the Freundlich constant related to the adsorption affinity; and n is a dimensionless indicator related to the adsorbent surface heterogeneity.

The Dubinin-Radushkevich (D-R) isotherm model was used to determine whether the nature of the process of adsorption is physical or chemical^{7, 8}. The equation of the D-R isotherm is expressed by eq (6).

$$\ln q_e = \ln Q_0 - \beta \varepsilon^2 \quad (6)$$

Where q_e ($\text{mg}\cdot\text{g}^{-1}$) is the amount of adsorbed Se per unit mass of the OV-CoO/CeO₂ composite material; Q_0 ($\text{mg}\cdot\text{g}^{-1}$) denotes the maximum adsorption capacity; β represents the activity coefficient related to the mean free energy of adsorption (mol^2/J^2); and ε is the Polanyi potential ($\varepsilon = RT\ln(1 + 1/C_e)$). The calculated q_m

and β are listed in Table S5. The mean free energy of adsorption E (kJ/mol) is expressed by eq (7):

$$E = \frac{1}{\sqrt{2\beta}} \quad (7)$$

According to the former reports, the adsorption mechanism can be determined by the value of E . When the values of E between 8 to 16 kJ/mol, the process of adsorption belongs to chemical adsorption⁹.

In HSDM, the adsorbent particle is assumed as a sphere which is surrounded by a stagnant liquid boundary layer, and the adsorbed adsorbate molecules are supposed to transport through diffusion on the surface of pore within the adsorbent particles¹⁰. In addition, during the migration process, it is assumed that a local equilibrium is established instantaneously between the adsorbate in the pore fluid and the adsorbate on the pore surface¹¹. The rate data can be used to calculate the C data value at different time t to determine the surface diffusion coefficient, which is expressed as eq(8):

$$C_{\text{data}} = \frac{Ct - Ce}{C_0 - Ce} \quad (8)$$

The value of t -bar can be calculated by the eq(9):

$$t_{\text{bar}} = D_s \frac{t}{R^2} \quad (9)$$

The Excel solver is used to find the optimal D_s/R^2 value by minimizing the objective function as shown in the eq(10):

$$OF = \sqrt{\frac{\sum_{i=1}^n \left(\frac{C_{\text{data},i} - C_{\text{model},i}}{C_{\text{data},i}} \right)^2}{n-1}} \quad (10)$$

The equation of the general empirical relationship is expressed by eq(11), which expresses the dimensionless concentration as a function of dimensionless time.

$$C = A_0 + A_1 (\ln t) + A_2 (\ln t)^2 + A_3 (\ln t)^3 \quad (11)$$

According to Freundlich model, the Freundlich constant related to the adsorption affinity K_F ($\text{mg/g} \cdot (\text{L/mg})^{1/n}$) is 10.45 and the dimensionless indicator related to the adsorbent surface heterogeneity $1/n$

is

0.49.

Text S4

In this study, the turnover frequency (TOF (s^{-1})) was used to measure the amount of oxidized sulfite per mol of Co atom per second¹. The amount of active substance in this study was determined by the content of active component in catalyst. The TOF was calculated as follows:

$$TOF = \frac{n_{S(VI)}}{n_{active} \times t} \quad (12)$$

Where $n_{S(VI)}$ (mol) is the amount of sulfate in oxidation products; n_{active} (mol) is the content of metal active component on catalyst and t (s) is the reaction time.

Text S5

The material cost in the reported literatures was calculated as follows:

$$C = \frac{\sum_{i=1}^n m_{\text{precursor}, i} \times c_{\text{precursor}, i}}{m_{\text{adsorbent}} \times q_e} \quad (13)$$

Where C ($\text{\$}\cdot\text{t}^{-1}$) is cost of adsorbent required for each ton of Se; i is one of the precursors contained in the material; $m_{\text{precursor}}$ (g) is the required mass of the precursor; $c_{\text{precursor}}$ ($\text{\$}\cdot\text{t}^{-1}$) is the price per ton of the precursor; $m_{\text{adsorbent}}$ (g) is the mass of the prepared adsorbent; q_e ($\text{mg}\cdot\text{g}^{-1}$) is the amount of adsorbed Se per unit mass of the adsorbent material.

Text S6

The synergistic catalytic/adsorption experiments were performed in simulated WFGD slurry to investigate the S/Se selectivity of OV-CoO/CeO₂. The S selectivity (S_s) and Se selectivity (S_{Se}) are calculated as follows:

$$S_s = \frac{TOF_{SW}}{TOF_{C/A}} \quad (14)$$

Where TOF_{SW} is the turnover frequency of OV-CoO/CeO₂ for SO₃²⁻ oxidation in simulated WFGD slurry with impurities. $TOF_{C/A}$ is the turnover frequency of OV-CoO/CeO₂ for SO₃²⁻ oxidation under simultaneous SO₃²⁻ catalytic oxidation and Se adsorption in pure environment.

$$S_{Se} = \frac{R_{SW}}{R_{C/A}} \quad (15)$$

Where R_{SW} is the Se removal efficiency of OV-CoO/CeO₂ in simulated WFGD slurry with impurities. $R_{C/A}$ is the Se removal efficiency of OV-CoO/CeO₂ under simultaneous SO₃²⁻ catalytic oxidation and Se adsorption in pure environment.

Figures

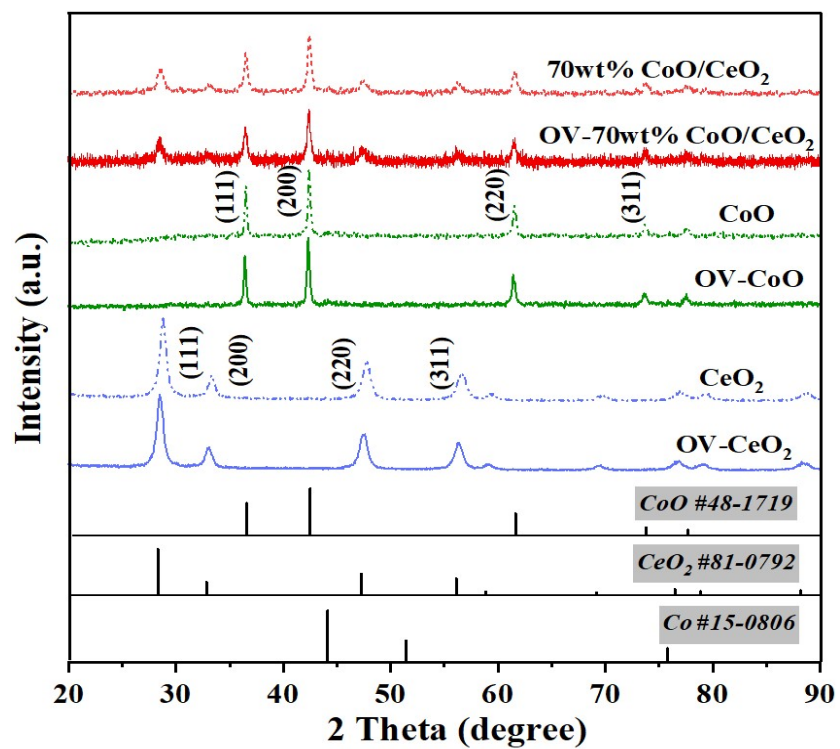


Fig. S1. XRD patterns of CoO, OV-CoO, CeO₂, OV-CeO₂, CoO/CeO₂ and OV-CoO/CeO₂ catalysts.

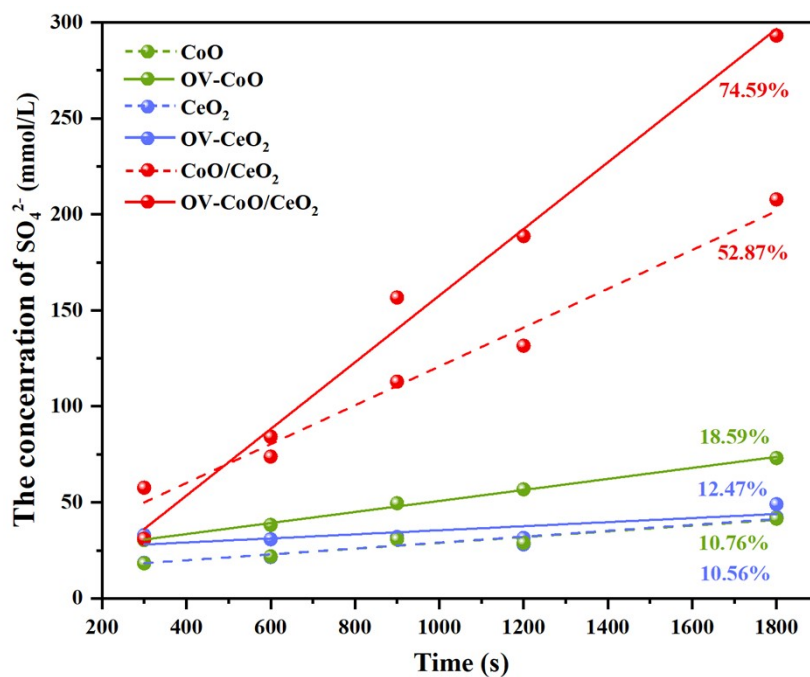


Fig. S2. Kinetics and efficiencies of sulfite oxidation by using CoO, CeO₂, CoO/CeO₂ materials with and without OV. General conditions: $c_{\text{cat}} = 0.5 \text{ g/L}$, $c_{(\text{NaSO}_3)} = 2 \text{ g/L}$, $P_{\text{O}_2} = 0.21 \text{ atm}$, $T = 318 \text{ K}$, and $\text{pH} = 8.0$.

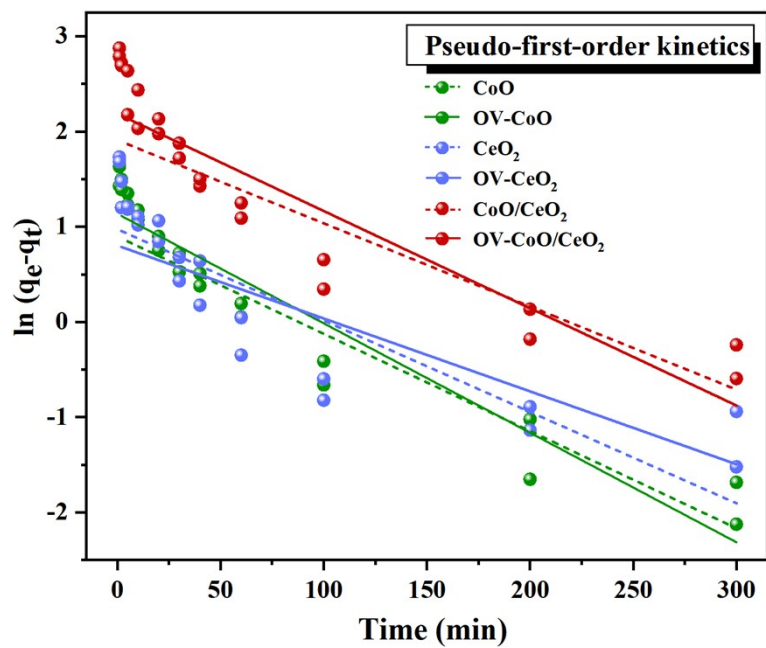


Fig. S3. Pseudo-first-order kinetics fitting curve for selenium adsorption.

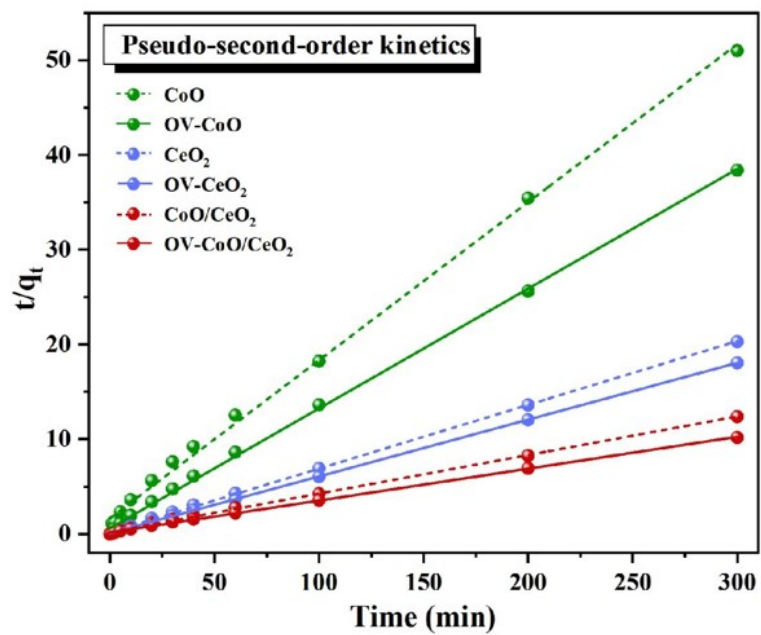


Fig. S4. Pseudo-second-order kinetics fitting curve for selenium adsorption.

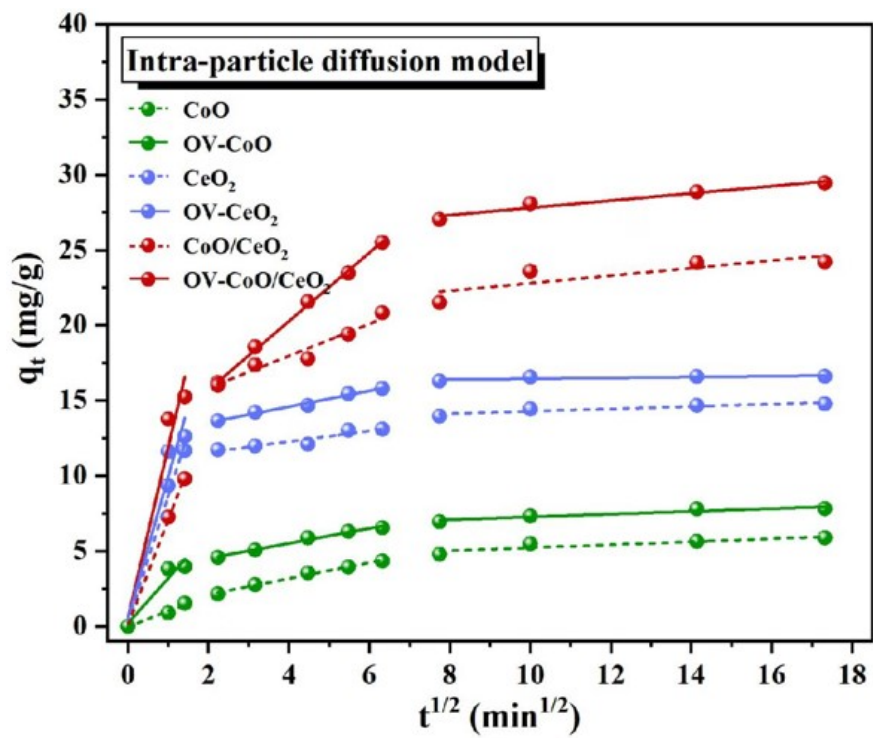


Fig. S5. Intra-particle diffusion model fitting curve for selenium adsorption.

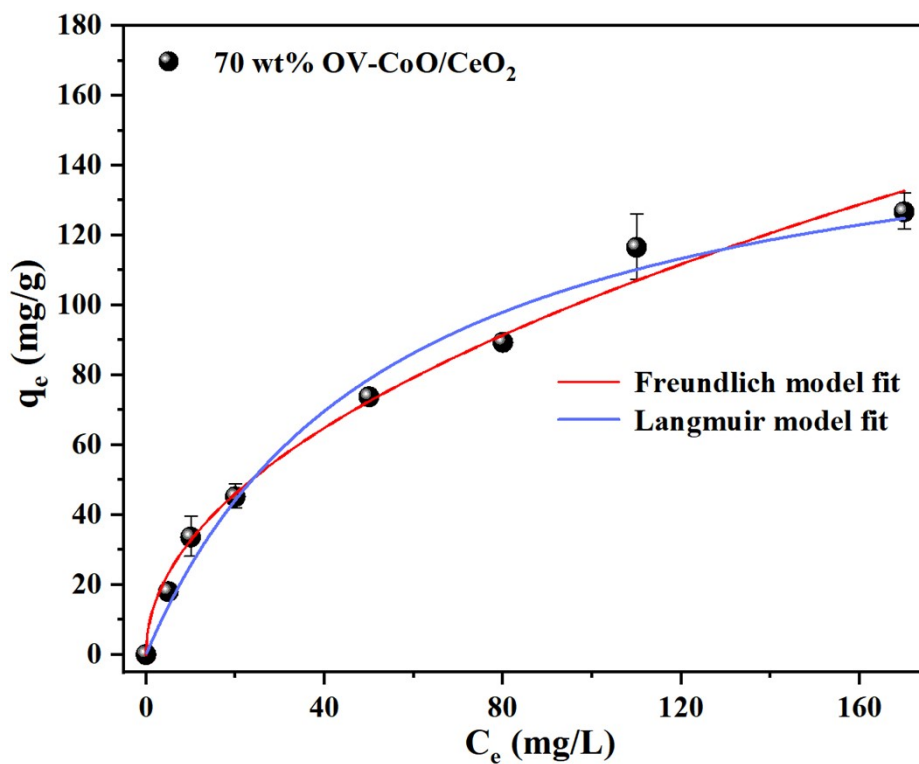


Fig. S6. Langmuir and Freundlich isotherm fitting parameters models for Se adsorption on OV-CoO/CeO₂.

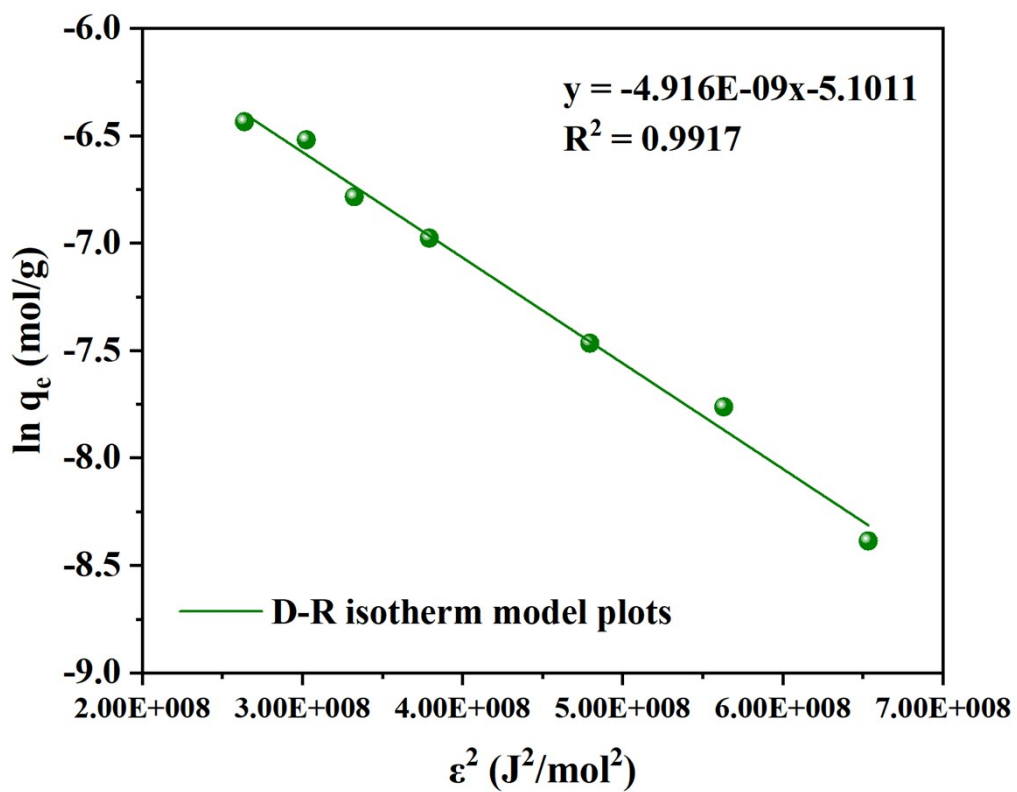


Fig. S7. Dubinin-Radushkevich model parameters for Se adsorption onto 70 wt% OV-CoO/CeO₂.

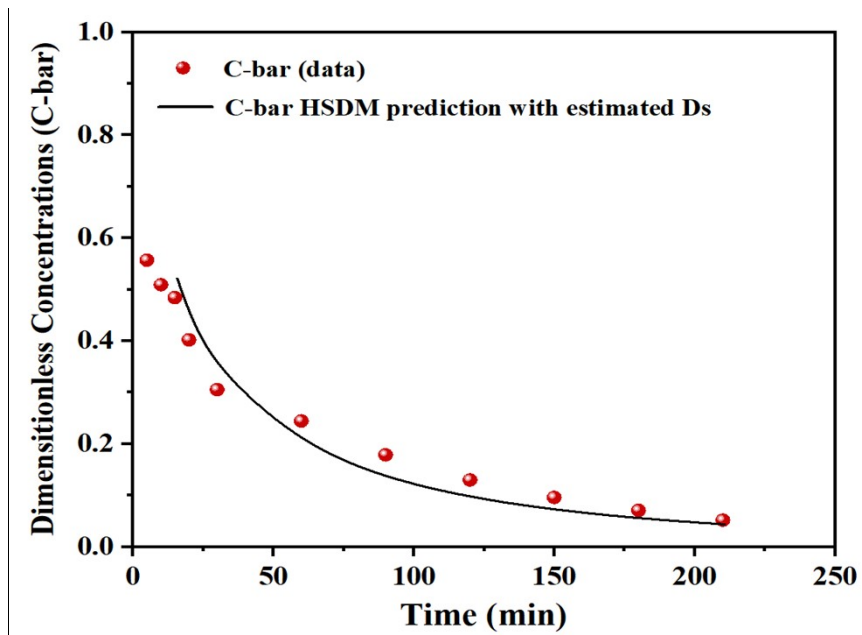


Fig. S8. Experimental data and HSDM prediction calculated by using D_s .

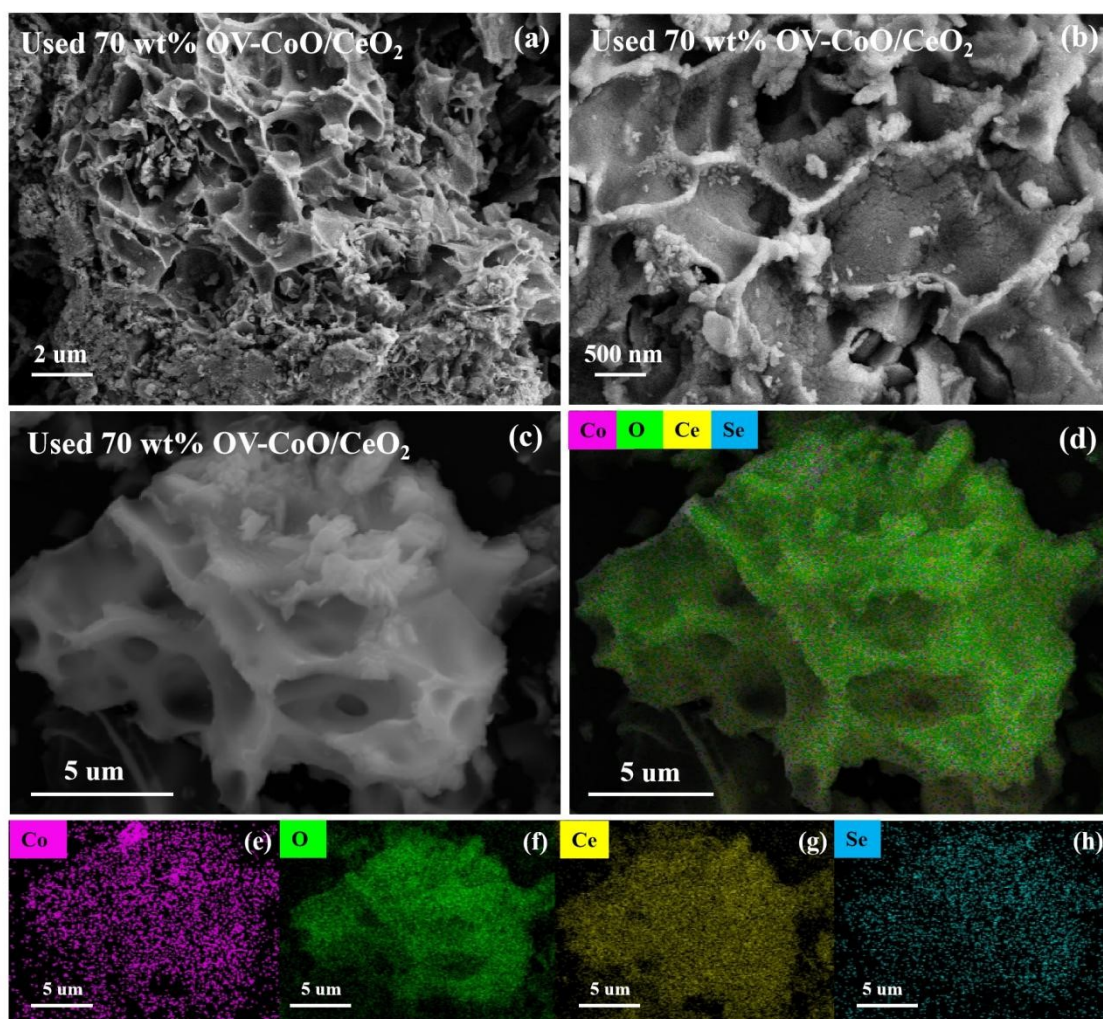


Fig. S9. SEM images and elemental mapping of the used OV-CoO/CeO₂

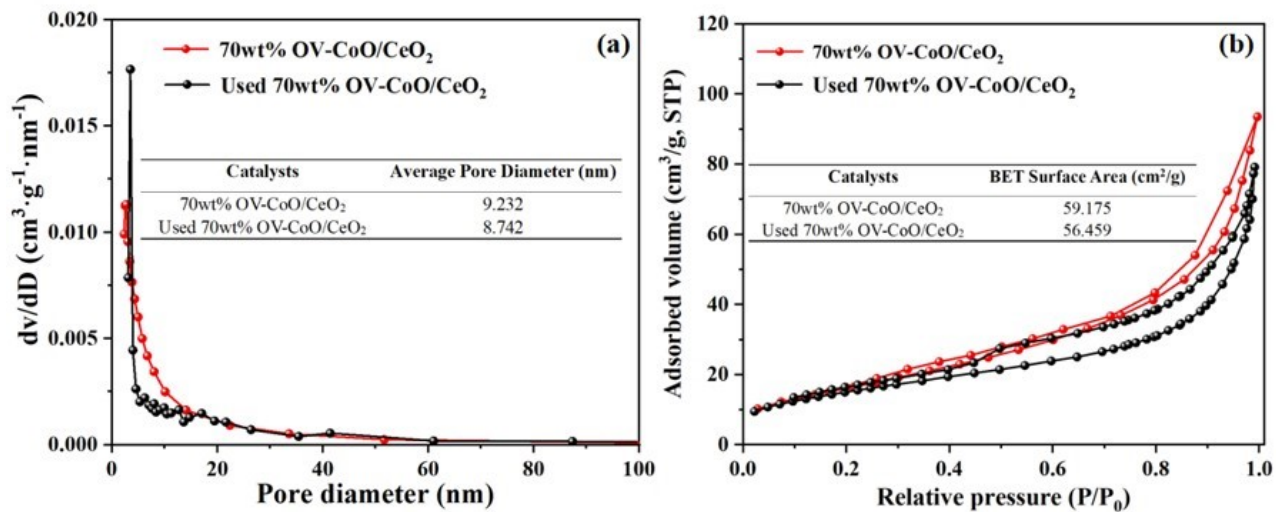


Fig.S10. (a) Pore diameter distribution of the used OV-CoO/CeO₂ (b) Nitrogen adsorption-desorption isotherms of the used OV-CoO/CeO₂

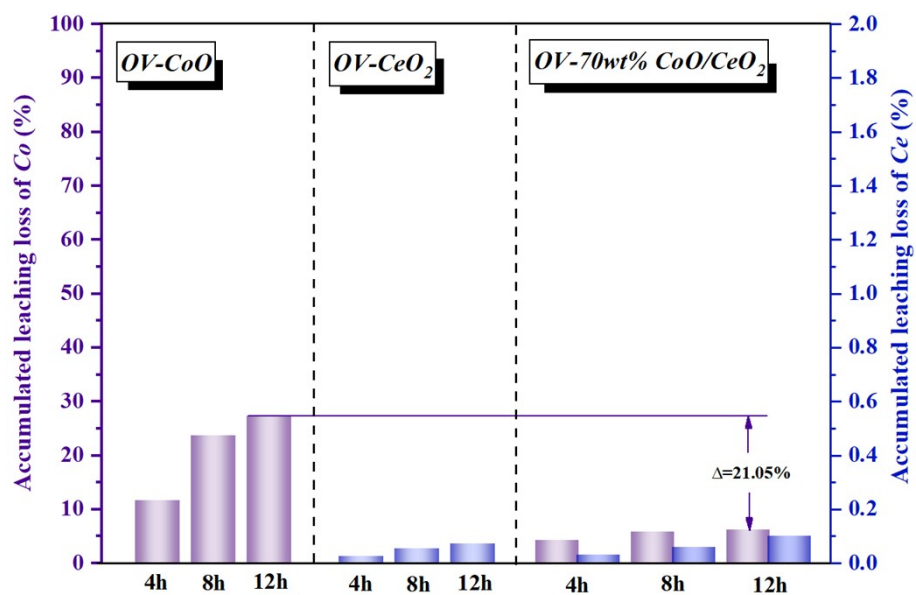


Fig. S11. Comparison of Co and Ce losses in sulfite oxidation by using CoO, CeO₂, CoO/CeO₂.

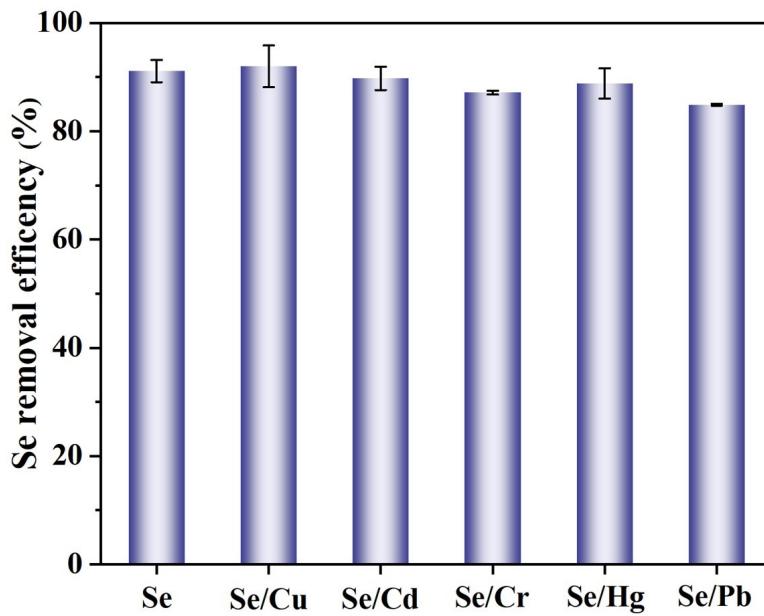


Fig. S12. Effects of coexisted toxic metals on selenium removal efficiency. $c_{Cr}=5$ mg/L, $c_{Cu}=0.5$ mg/L, c_{Hg}
 $= 0.2$ mg/L, $c_{Pb} = c_{Se}$ 1mg/L, $c_{Cd} = 0.1$ mg/L.

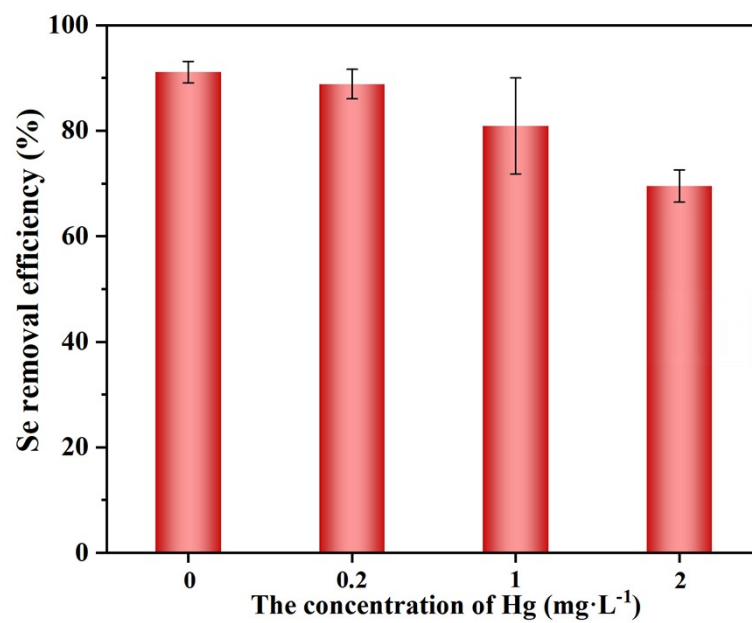


Fig. S13. Effect of Hg on Se adsorption

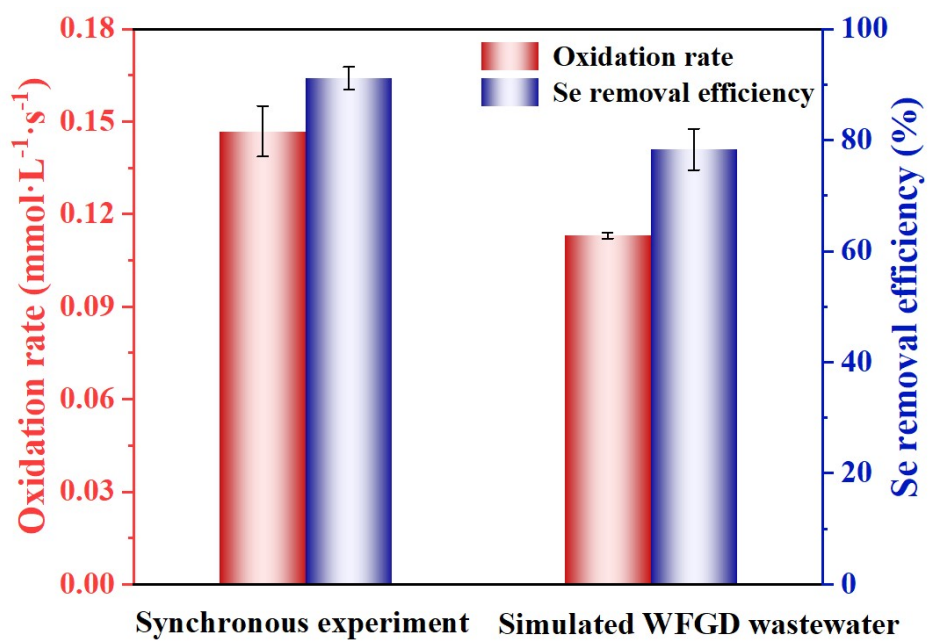


Fig. S14. Catalytic/adsorption performance of OV-CoO/CeO₂ in simulated WFGD wastewater

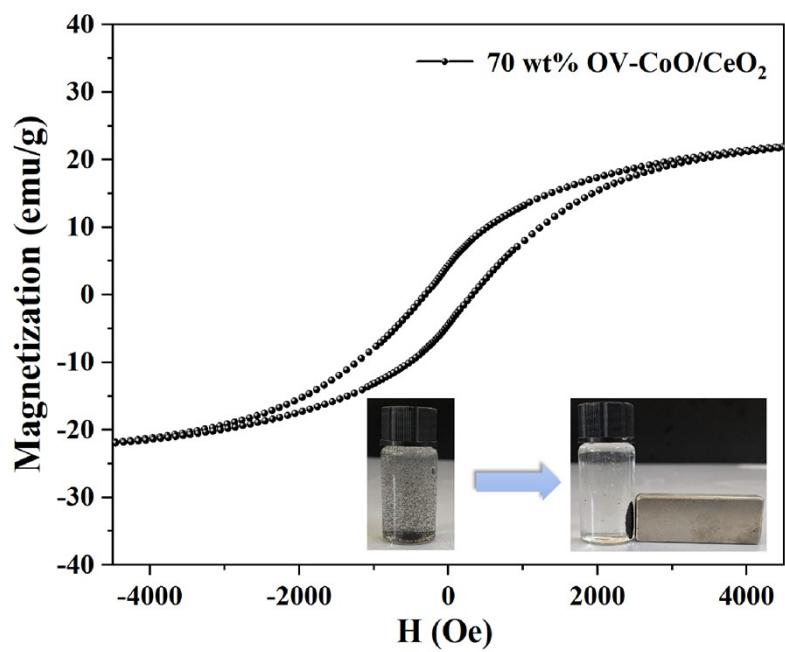


Fig. S15. M-H hysteresis curves of the 70 wt% OV-CoO/CeO₂ catalyst.

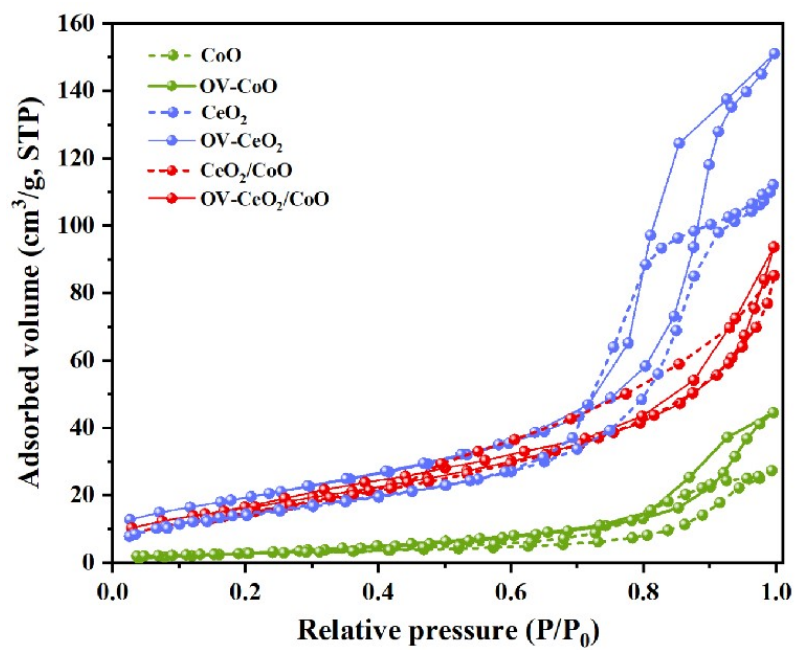


Fig. S16. Nitrogen adsorption-desorption isotherms of the different materials.

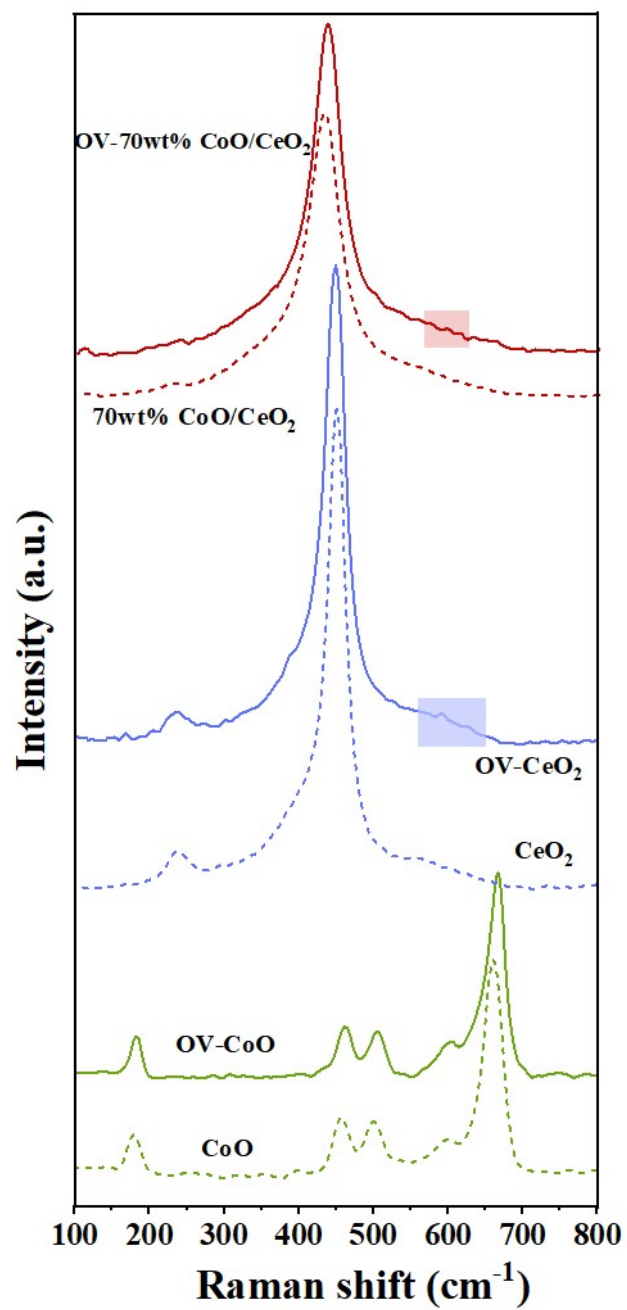


Fig. S17. Raman spectra of CoO, CeO₂, CoO/CeO₂ materials with and without OV.

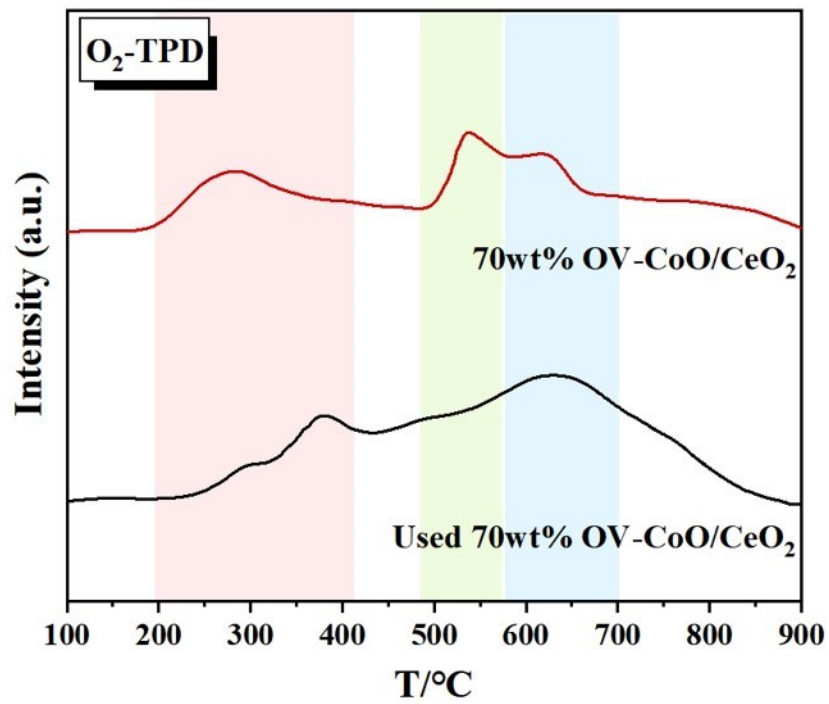


Fig.S18. Comparison of the TPD profiles between used OV-CoO/CeO₂ and fresh OV-CoO/CeO₂

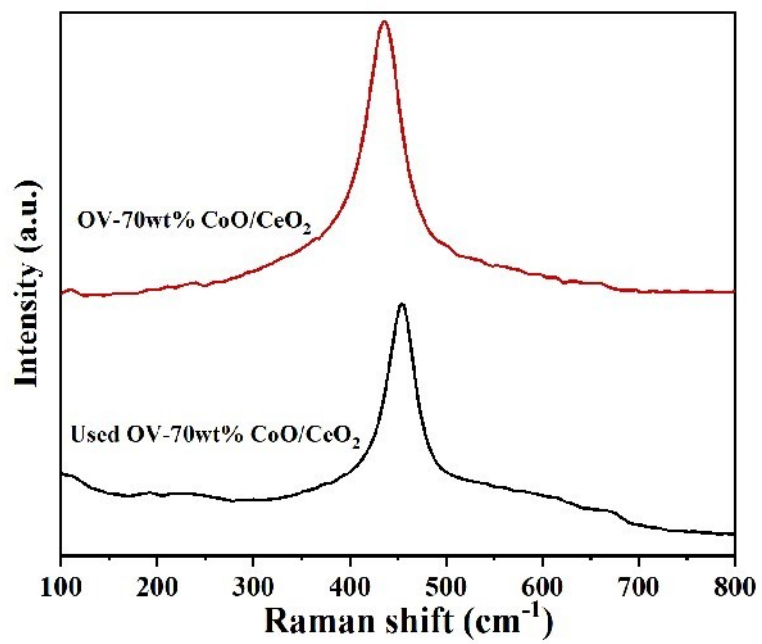


Fig. S19. Comparison of the Raman spectra between used OV-CoO/CeO₂ and fresh OV-CoO/CeO₂

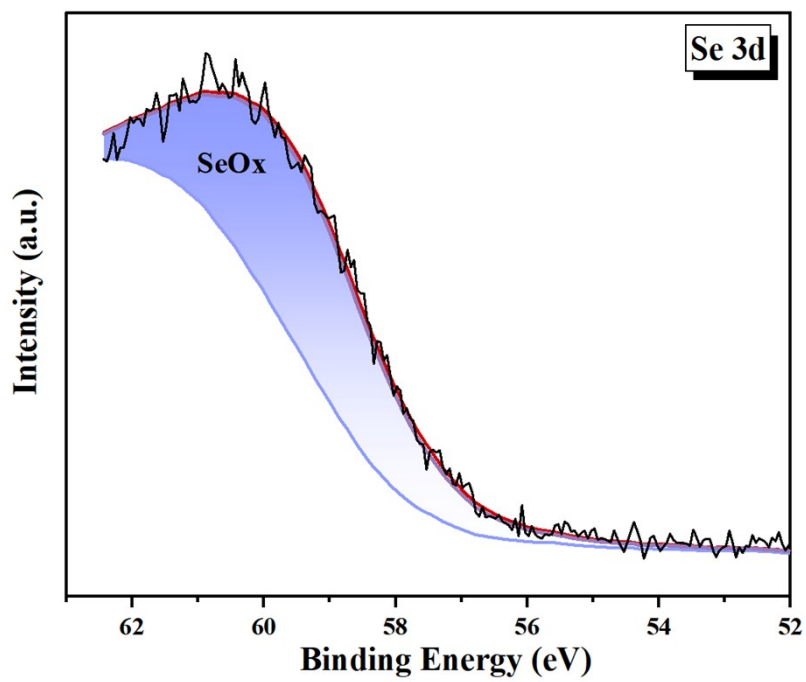


Fig. S20. Se 3d XPS spectra of OV-CoO/CeO₂ after Se adsorption.

Tables

Table S1 Comparison of the TOF for other Co-based catalysts

Catalysts	Catalyst dosage (g·L ⁻¹)	Co concentration (wt.%)	Oxidation rate of SO ₃ ²⁻ (mmol·L ⁻¹ ·s ⁻¹)	TOF (s ⁻¹)	References
Mn@ZIF67	0.50	18.07	0.077	0.014	12
Co/C₃N₄	0.50	24.10	0.074	0.010	13
Co-MOF-74	0.50	29.59	0.081	0.009	14
Co₃O₄-NPs@KIT-6	1.00	4.00	0.0902	0.038	15
BISC	1.00	13.32	0.1446	0.018	16
Co-MCM-48	0.50	5.90	0.074	0.042	17
OV-CoO/CeO₂	0.25	24.02	0.174	0.050	This work

Table S2. Parameters of adsorption kinetics for Se adsorption.

		Composites					
		CoO	OV-CoO	CeO ₂	OV-CeO ₂	CoO/CeO ₂	OV-CoO/CeO ₂
Pseudo- first -order	$q_{e, cal}(mg \cdot g^{-1})$	3.004	3.561	3.034	3.010	7.389	9.974
	$k_1 \times 10^2 (min^{-1})$	1.021	1.149	0.959	0.765	0.873	1.102
	R^2	0.907	0.934	0.890	0.676	0.855	0.890
Pseudo- second -order	$q_{e, cal}(mg \cdot g^{-1})$	6.024	7.936	14.925	16.949	24.570	33.333
	$k_2 \times 10^{-2} (g \cdot (mg \cdot min)^{-1})$	1.664	2.633	2.747	4.455	0.899	0.734
	R^2	0.997	0.999	0.999	0.999	0.999	0.999
Intra- Particle diffusion model	$k_1 (mg \cdot g^{-1} \cdot min^{-1/2})$	1.046	3.002	8.458	9.423	6.994	11.323
	R^2	0.981	0.936	0.990	0.954	0.999	0.960
Particle diffusion model	$k_2 (mg \cdot g^{-1} \cdot min^{-1/2})$	0.533	0.495	0.359	0.526	1.063	2.277
	R^2	0.990	0.985	0.891	0.986	0.943	0.997
	$k_3 (mg \cdot g^{-1} \cdot min^{-1/2})$	0.099	0.092	0.080	0.028	0.250	0.240
	R^2	0.822	0.887	0.849	0.640	0.705	0.955

Table S3. Comparison of adsorbents for Se in reported literatures

Adsorbents	Adsorbent dosage (g·L⁻¹)	Materials cost estimation (\$·t⁻¹)	Adsorption capacity (mg·g⁻¹) for Se	Adsorbent cost required for each ton of Se (\$·t⁻¹)	Reference
CuFe₂O₄	0.40	5344.8	14.10	379063.8	17
CoFe₂O₄	0.40	9699.9	11.60	836198.3	17
MnFe₂O₄	0.40	2842.9	3.90	728948.7	17
BC-ZVI	0.50	24757.9	62.52	395999.7	18
MGO	1.00	8002817	23.81	336111591.8	19
UiO-66-NH₂	0.50	122916.6	26.80	4586440.3	20
MGO-PAA	0.015	17842285.1	120.10	148561907.6	21
OV-CoO/CeO₂	0.25	22767.4	126.70	179695.3	This work

Table S4. Langmuir and Freundlich isotherm fitting parameters for Se adsorption on OV-CoO/CeO₂.

Composite	Langmuir			Freundlich			
	$q_m(\text{mg}\cdot\text{g}^{-1})$	Actual $q_m(\text{mg}\cdot\text{g}^{-1})$	$K_L(\text{L}\cdot\text{mg}^{-1})$	R^2	$K_F(\text{mg}^{1-\frac{1}{n}}\text{L}^{\frac{1}{n}}\text{g}^{-1})$	R^2	n
OV-CoO/CeO ₂	175.454	126.701	0.016	0.971	10.452	0.992	2.021

Table S5. Dubinin-Radushkevich isotherm fitting parameters for Se adsorption on OV-CoO/CeO₂.

Composite	D-R model			
	Q_0 (mol·g ⁻¹)	β (mol ² ·J ⁻²)	E (kJ·mol ⁻¹)	R ²
OV-CoO/CeO ₂	6.090E-3	4.916E-9	10.085	0.992

Table S6. Parameters used for the empirical equation that describe solutions to the HSDM for a batch reactor for Freundlich adsorption intensity parameters ($1/n$)

Composite	HSDM		Empirical Equation $C=A_0 + A_1 (\ln t)+A_2 (\ln t)^2+A_3 (\ln t)^3$					
	$K_L (\text{mg} \cdot \text{g}^{-1}) \cdot (\text{L} \cdot \text{mg}^{-1})^{1/n}$	$D_s (\text{cm}^2 \cdot \text{s}^{-1})$	Freundlich adsorption intensity parameter ($1/n$)	C_e/C_0	A_0	A_1	A_2	A_3
OV-CoO/CeO ₂	10.45	4.17E-13	0.4948	0.1	0.1139	0.1536	3.53E-3	5.30E-5

Table S7. Calculating Ds using mathematical solution to the HSDM

t/min	Ct/C0	Ct	t-bar	$\frac{Ct - Ce}{C_{data} = C0 - Ce}$	C model	$(\frac{C_{data} - C_{model}}{C_{data}})^2$
5	0.595408529	5060972.5	2.10E-03	0.557054675	0.889025371	3.55E-01
10	0.551634118	4688890	4.19E-03	0.509130603	0.644416766	7.06E-02
15	0.529052353	4496945	6.29E-03	0.484408166	0.519404777	5.22E-03
20	0.453954118	3858610	8.39E-03	0.402190881	0.438890893	8.33E-03
30	0.365555588	3107222.5	1.26E-02	0.305412481	0.337050066	1.07E-02
60	0.309836471	2633610	2.52E-02	0.244411386	0.194835346	4.11E-02
90	0.249755	2122917.5	3.77E-02	0.178634402	0.130519284	7.25E-02
120	0.205196176	1744167.5	5.03E-02	0.129851558	0.093427673	7.87E-02
150	0.174182941	1480555	6.29E-02	0.095898377	0.069574592	7.53E-02
180	0.151241765	1285555	7.55E-02	0.070782457	0.053291431	6.11E-02
210	0.133872647	1137917.5	8.80E-02	0.051766808	0.041783463	3.72E-02

Table S8. Flue Gas Desulfurization Wastewater Characteristics

Parameter	Typical influent range (mg·L⁻¹)	References
Cadmium (Cd)	0.05-0.1	23, 24
Chromium (Cr)	0.3-1	24, 25
Mercury (Hg)	0.01-0.8	26, 27
Lead (Pb)	0.5-1.5	25
Copper (Cu)	0.2-0.8	28
Magnesium (Mg)	50-4000	28
Chloride (Cl)	10000-25000	29
Nitrate (NO ₃)	30-120	26
Selenium (Se)	1-4	24, 26, 29

Table S9. Pore diameter, pore volume and BET surface area of the different materials.

Catalysts	Average Pore Diameter (nm)	Pore Volume (cm³/g)	BET Surface Area (cm²/g)
CoO	21.348	0.067	12.638
OV-CoO	15.958	0.0428	10.729
CeO ₂	12.227	0.174	57.032
OV-CeO ₂	12.959	0.231	71.215
70wt% CoO/CeO ₂	8.771	0.123	56.206
70wt% OV-CoO/CeO ₂	9.232	0.137	59.175

Table S10. Ratios of Co, Ce, and O species on the surface of five different kinds of catalysts.

Sample	Co 2p		Ce 3d		O 1s		
	Co ²⁺ /Co	Co ⁰ /Co	Ce ³⁺ /Ce	Ce ⁴⁺ /Ce	O _α /O	O _β /O	O _Γ /O
10 wt% OV-CoO/CeO ₂	87.42%	12.58%	21.27%	78.73%	44.13%	47.13%	8.74%
30 wt% OV-CoO/CeO ₂	87.40%	12.60%	24.87%	75.13%	33.78%	52.52%	13.70%
50 wt% OV-CoO/CeO ₂	87.05%	12.95%	29.00%	71.00%	24.71%	59.52%	15.77%
70 wt% OV-CoO/CeO ₂	87.66%	12.33%	40.77%	59.23%	22.33%	67.48%	10.62%
90 wt% OV-CoO/CeO ₂	80.41%	19.69%	20.69%	79.31%	32.63%	55.74%	11.63%

Table S11. Ratios of Co, Ce, and O species on the surface of OV-CoO/CeO₂ before and after catalysis/adsorption.

Sample	Co 2p		Ce 3d		O 1s		
	Co ²⁺ /Co	Co ⁰ /Co	Ce ³⁺ /Ce	Ce ⁴⁺ /Ce	O _α /O	O _β /O	O _Γ /O
OV-CoO/CeO ₂	87.66%	12.33%	40.77%	59.23%	22.33%	67.48%	10.62%
OV-CoO/CeO ₂ after catalysis	93.63%	6.37%	38.71%	61.29%	35.77%	64.54%	0.69%
OV-CoO/CeO ₂ after adsorption	90.04%	9.96%	34.45%	65.56%	50.05%	47.09%	2.86%

References

1. L. D. Wang, T. Y. Qi, S. Y. Wu, S. H. Zhang, D. Qi and H. N. Xiao, *Journal of Materials Chemistry A*, 2017, **5**, 8018-8028.
2. M. Badruzzaman, P. Westerhoff and D. R. U. Knappe, *Water Res.*, 2004, **38**, 4002-4012.
3. X. P. Min, D. Trujillo, J. W. Huo, Q. Q. Dong and Y. Wang, *Chem. Eng. J.*, 2020, **396**.
4. K. Gupta and U. C. Ghosh, *J. Hazard. Mater.*, 2009, **161**, 884-892.
5. C. H. Liu, Y. H. Chuang, T. Y. Chen, Y. Tian, H. Li, M. K. Wang and W. Zhang, *Environ. Sci. Technol.*, 2015, **49**, 7726-7734.
6. X. Jin, Y. Duan, D. P. Liu, X. L. Feng, W. Li, Z. Zhang and Y. Zhang, *Acs Applied Nano Materials*, 2019, **2**, 5769-5778.
7. K. X. Fu, X. Liu, C. Y. Lv, J. M. Luo, M. X. Sun, S. L. Luo and J. C. Crittenden, *Environ. Sci. Technol.*, 2022, **56**, 2677-2688.
8. J. M. Luo, M. Sun, C. L. Ritt, X. Liu, Y. Pei, J. C. Crittenden and M. Elimelech, *Environ. Sci. Technol.*, 2019, **53**, 2075.
9. J. Luo, X. Luo, J. Crittenden, J. Qu, Y. Bai, Y. Peng and J. Li, *Environ. Sci. Technol.*, 2015, **49**, 11115-11124.
10. Q. Zhang, J. Crittenden, K. Hristovski, D. Hand and P. Westerhoff, *Water Res.*, 2009, **43**, 1859-1866.
11. M. Usman, M. Zarebanadkouki, M. Waseem, I. A. Katsoyiannis and M. Ernst, *J. Hazard. Mater.*, 2020, **400**, 123221.
12. L. Xing, J. Liu, T. Qi, L. Wang, Z. Wang and S. Zhang, *Applied Catalysis B-Environmental*, 2020, **275**.
13. M. Li, T. Qi, R. Yang, H.-N. Xiao, Z. Fang, S. A. Hodge, T. D. James, L. Wang and B. Mao, *Journal*

of Materials Chemistry A, 2018, **6**, 11296-11305.

14. M. Li, Q. Guo, L. Xing, L. Yang, T. Qi, P. Xu, S. Zhang and L. Wang, *Journal of Colloid and Interface Science*, 2020, **559**, 88-95.
15. T. Y. Qi, L. D. Wang, Y. G. Wang, L. Xing, L. Zhang, J. Liu, H. N. Xiao and S. H. Zhang, *Environ. Sci. Technol.*, 2019, **53**, 13477-13485.
16. T. Y. Qi, L. Xing, Z. M. Fang, L. Zhang, H. N. Xiao and L. D. Wang, *Journal of Materials Chemistry A*, 2021, **9**, 13288-13296.
17. L. Wang, L. Xing, J. Liu, T. Qi, S. Zhang, Y. Ma and P. Ning, *Chem. Eng. J.*, 2021, **407**.
18. W. Sun, W. Pan, F. Wang and N. Xu, *Chem. Eng. J.*, 2015, **273**, 353-362.
19. G. Tan, Y. Mao, H. Wang, M. Junaid and N. Xu, *Environmental Science and Pollution Research*, 2019, **26**, 21609-21618.
20. Y. Fu, J. Wang, Q. Liu and H. Zeng, *Carbon*, 2014, **77**, 710-721.
21. J. Wei, W. Zhang, W. Pan, C. Li and W. Sun, *Environmental Science-Nano*, 2018, **5**, 1441-1453.
22. Z. Lu, J. Yu, H. Zeng and Q. Liu, *Separation and Purification Technology*, 2017, **183**, 249-257.
23. L. C. Staicu, N. Morin-Crini and G. Crini, *Chemosphere*, 2017, **172**, 111-119.
24. W. L. Zhang, H. Oswal, J. E. Renew, B. Gallagher, K. Ellison and C. H. Huang, *J. Hazard. Mater.*, 2020, **384**.
25. F. Franco, M. Benitez-Guerrero, I. Gonzalez-Trivino, R. Perez-Recuerda, C. Assiego, J. Cifuentes-Melchor and J. Pascual-Cosp, *Appl. Clay Sci.*, 2016, **119**, 321-332.
26. Y. H. Huang, P. K. Peddi, C. Tang, H. Zeng and X. Teng, *Separation and Purification Technology*, 2013, **118**, 690-698.
27. S. Zhao, D. Pudasainee, Y. Duan, R. Gupta, M. Liu and J. Lu, *Progress in Energy and Combustion*

Science, 2019, **73**, 26-64.

28. P. Cordoba, O. Font, M. Izquierdo, X. Querol, C. Leiva, M. A. Lopez-Anton, M. Diaz-Somoano, R. Ochoa-Gonzalez, M. R. Martinez-Tarazona and P. Gomez, *Fuel*, 2012, **102**, 773-788.
29. C.-M. Cheng, P. Hack, P. Chu, Y.-N. Chang, T.-Y. Lin, C.-S. Ko, P.-H. Chiang, C.-C. He, Y.-M. Lai and W.-P. Pan, *Energy Fuels*, 2009, **23**, 4805-4816.